Electronic structure investigation of a charge density wave coupled to a metal-to-metal transition in $Ce_3Co_4Sn_{13}$

A. Singh,[1] H. Y. Huang,[1] Y. Y. Chin,[1,2] Y. F. Liao,[1] T. C. Huang,[1,3] J. Okamoto,[1] W. B. Wu,[1] H. J. Lin,[1] K. D. Tsuei,[1] R. P. Wang,[4] F. M. F. de Groot,[4] C. N. Kuo,[5] H. F. Liu,[5] C. S. Lue,[5] C. T. Chen,[1] D. J. Huang,[1,3] and A. Chainani[1]

[1]*National Synchrotron Radiation Research Center, Hsinchu 30076, Taiwan*

[2]*Department of Physics, National Chung Cheng University, Chiayi 62102, Taiwan*

[3]*Department of Electrophysics, National Chiao Tung University, Hsinchu 30010, Taiwan*

[4]*Inorganic Chemistry and Catalysis, Utrecht University, Universiteitsweg 99, 3584 CG Utrecht, The Netherlands*

[5]*Department of Physics, National Cheng Kung University, Tainan 70101, Taiwan*

(Received 25 June 2018; revised manuscript received 21 November 2018; published 18 December 2018)

We study the electronic structure of the skutterudite $Ce_3Co_4Sn_{13}$, which is known to exhibit a charge density wave (CDW) transition, at temperature $T_{CDW} \sim 160$ K, coupled to a metal-to-metal transition. We use temperature dependent hard x-ray photoemission spectroscopy (HAXPES) and x-ray absorption spectroscopy (XAS) to investigate the occupied and unoccupied electronic states of $Ce_3Co_4Sn_{13}$. The Co $2p$ and Sn $3p$ core level spectra show small but finite shifts in binding energy positions across T_{CDW} while Ce $3d$ core level spectra do not show any change across the transition. The Ce $M_{4,5}$-edge XAS spectrum compared with calculations indicate a typical trivalent ionic Ce^{3+} spectral shape, ruling out Kondo screening in $Ce_3Co_4Sn_{13}$. In contrast, the Co $L_{2,3}$-edge XAS spectrum compared with a calculated spectrum shows evidence for hybridization with neighboring Sn atoms in a trigonal prismatic co-ordination. Temperature dependent XAS across the Co $L_{2,3}$-edge shows a small shift across T_{CDW}, consistent with HAXPES results. Detailed XAS measurements as a function of temperature show that the spectral shifts occur with a hysteresis across T_{CDW}, indicative of a first-order transition. Valence band spectra show a normal Fermi edge above and below T_{CDW}. The Co $3d$ states are observed at a binding energy of $\sim$2 eV while the Ce $4f$ states occur as a weak feature within 0.5 eV of the Fermi level. The results suggest an unusual CDW transition coupled to a metal-to-metal transition in $Ce_3Co_4Sn_{13}$.

DOI: 10.1103/PhysRevB.98.235136

I. INTRODUCTION

Since the original work on the theoretical prediction of charge density wave (CDW) transitions by Peierls [1], and its experimental confirmation in quasi-one-dimensional (1D) materials [2,3] like $K_{0.3}MoO_3$ and $NbSe_3$, the CDW transition has continued to fascinate our understanding of temperature dependent phase transitions [4]. While the early work concentrated on quasi-1D crystal structures [2,3], subsequent studies showed that charge density wave order, or more generally, charge ordering transitions, can occur in quasi-2D as well as 3D materials [4–12]. Charge ordering occurs in a variety of materials such as quasi-2D transition metal dichalcogenides (like $NbSe_2$, $TiSe_2$, TaS_2, $TaSe_2$, etc.) [5–9] and 3D oxide systems (like $BaBiO_3$, $RNiO_3$, $La_{1-x}Ca_xMnO_3$, etc.) [10–12]. Further, charge ordering transitions have recently attracted significant attention in high-T_c copper-oxide superconductors [13–15], as well as materials like RTe_3, R_2Te_5, and RTe_2 (R = rare-earth element) [16–21].

The valence and conduction band electronic states of the materials discussed above are derived from strongly correlated transition metal d-electron or rare-earth f-electron states, bonding with ligand electrons. It is noted that even for the nickel- and copper-based oxide families, which also contain rare-earth (R) metal cations like La, Nd, etc., the electronic states of the R ions are known to exhibit negligible contributions to the valence-band and conduction-band states near the Fermi level. However, there are other series of materials which exhibit CDW transitions and include both transition metal d and rare-earth f electrons. These are intermetallics such as the series $R_3M_4Sn_{13}$ (R = La, Ce, Pr, Nd, Gd, Yb; M = Co, Rh, Ir) [22–27]. The $R_3M_4Sn_{13}$ series includes materials which show low-T_c superconductivity coexisting with CDW transitions; for example, $La_3Co_4Sn_{13}$ shows low-T_c superconductivity below $T_c = 2.85$ K and a CDW transition at $T_{CDW} \sim 160$ K [22,24,26,27]. This behavior is reminiscent of 2H-$NbSe_2$, which shows superconductivity below $T_c = 7.2$ K and a CDW transition at $T_{CDW} \sim 35$ K [8]. In contrast, $Ce_3Co_4Sn_{13}$ shows heavy fermion behavior and a CDW transition at $T_{CDW} \sim 160$ K [22,24,25,27], but no superconductivity. So the natural question arises, What is the role of the rare-earth R ions and the transition metal M ions in the superconductivity/heavy-fermion behavior and the CDW transition. This is important because there are two more ternary series of compounds, namely $R_5M_4Si_{10}$ and RMC_2 (R is a rare-earth element and M is a transition metal), where metallicity is retained across CDW transitions.

Both the series $R_5M_4Si_{10}$ and RMC_2 also show charge density wave transitions (at T_{CDW}) with local moment behavior, and coexisting magnetic order and/or superconductivity at very low temperatures compared to T_{CDW}. For example, in the $R_5M_4Si_{10}$ series [28–32], $Er_5Ir_4Si_{10}$ shows an

incommensurate CDW transition at 155 K, followed by a commensurate CDW transition at 55 K, and local moment antiferromagnetic order below 2.8 K. In contrast, $Lu_5Ir_4Si_{10}$ shows a commensurate CDW transition at 80 K, followed by superconductivity below 3.9 K. More interestingly, the CDW transition temperatures as a function of R decrease linearly from Dy to Lu, except for Yb which does not show a CDW transition. It was shown that both ionic size and disorder effects play an important role in the CDW transitions in the $R_5M_4Si_{10}$ series [32]. On the other hand, in the $RNiC_2$ series [33,34] the CDW transition temperature shows a systematic increase in T_{CDW} from Ce to Lu, and magnetic ordering at low temperatures between 4 and 25 K, depending on the R ion. In the $RNiC_2$ series, Yb and La do not show a CDW transition, while only La shows superconductivity below 2.7 K. Interestingly, while all the remaining R ions show antiferromagnetic order, only $SmNiC_2$ shows ferromagnetic order below 17 K. A recent study discussed the role of the band structure changes associated with lanthanide contraction as a possible origin for the increase in T_{CDW} in the $RNiC_2$ series [34]. Hence, there are two more series of ternary rare-earth-containing compounds, which show metallicity across CDW transitions and local moment behavior, in contrast to the normal expectation of a metal-to-insulator transition accompanying a CDW transition [4].

In this work, we study the electronic structure changes across the CDW transition in the ternary intermetallic compound $Ce_3Co_4Sn_{13}$ using a combination of bulk-sensitive hard x-ray photoelectron spectroscopy (HAXPES) and x-ray absorption spectroscopy (XAS). Early studies revealed an anomalous bump in the electrical resistivity of $Ce_3Co_4Sn_{13}$ around $T \sim 160$ K, but with metallic behavior above and below the anomaly [22–24]. It was also shown that $Ce_3Co_4Sn_{13}$ exhibits an increase below 5 K in the specific heat with a peak at 0.65 K. The authors estimated a specific heat coefficient $\gamma \sim 75$ mJ mol^{-1}K^{-1} as $T \to 0$, and it was 4280 mJ mol^{-1}K^{-1} at the peak [23]. They concluded that $Ce_3Co_4Sn_{13}$ is a heavy electron system exhibiting Kondo scattering and it undergoes a magnetic transition at 0.65 K. However, the magnetic susceptibility did not show any change at the high temperature resistivity anomaly at $T \sim 160$ K, and the high temperature susceptibility indicated a Ce^{3+} state with a $\mu_{\text{eff}} = 2.56\mu_B$, very close to the ionic Ce^{3+} value of $2.54\mu_B$.

Lue *et al.* predicted a CDW transition in $Ce_3Co_4Sn_{13}$ based on specific heat studies and nuclear magnetic resonance measurements as a function of temperature [25]. They based their picture on the absence of a magnetic transition across $T \sim 160$ K and the possibility of a structural transition driven by electron-lattice coupling. Further, the nuclear magnetic resonance (NMR) data were consistent with a reduced density of states in the low temperature phase, which suggested a partial Fermi surface gapping in the electronic structure. However, evidence for a structural transition or a superstructure could not be observed from conventional laboratory based diffraction experiments. This is mainly attributed to the fact that the crystal structure is quite complicated [23,27,35]. At room temperature, the structure crystallizes in the so-called $Yb_3Co_4Sn_{13}$ cubic structure (space group $Pm\bar{3}n$, no. 223), and it has a large unit cell with lattice parameter $a = 9.6022$ Å. It consists of Sn icosahedra, Ce-Sn cuboctahedra, and Co-Sn trigonal prisms. It is important to note that although the $CeSn_{12}$ cuboctahedrahave two types of Ce-Sn distances, they are both large: 3.4080 and 3.3335 Å [23]. Accordingly, Ce and Sn are expected to be weakly hybridized. In contrast, the $CoSn_6$ trigonal prisms exhibit a Co-Sn distance of 2.6210 Å [23], and are expected to be relatively strongly hybridized based on band structure calculations [36]. A synchrotron based hard x-ray diffraction study [27] revealed the formation of a superstructure below $T_{CDW} \sim 160$ K with wave vector $q = (1/2, 1/2, 0)$ confirming the CDW transition in the low temperature phase. In addition, the results [27] suggested a chiral cubic structure (space group $I2_13$, no. 199) for the CDW phase in $Ce_3Co_4Sn_{13}$. In a very recent inelastic neutron scattering study [37] it was shown that the Ce $4f$ crystal field excitation spectrum shows features at 6 and 29 meV, which remain essentially unaffected across T_{CDW}, suggesting that the Ce $4f$ electronic states do not participate in the transition. This is consistent with the fact that T_{CDW} is similar for $La_3Co_4Sn_{13}$ compared to $Ce_3Co_4Sn_{13}$ [25,26].

Surprisingly, there are only two photoemission spectroscopy studies reported to date on $R_3Co_4Sn_{13}$ (R = La, Ce; M = Co, Ru, and Rh) systems [38,39]. Both studies were carried out using relatively surface-sensitive soft x-ray photoelectron spectroscopy [38,39]. For $Ce_3Co_4Sn_{13}$, the authors could not find any changes in the Ce $4f$ and $3d$ states as well as in the Co $3d$ electronic states, and observed changes only in the Sn $4d$ core level spectra. Further, the Co $2p$ spectra were not reported in their studies. The results are surprising because, based on strong hybridization and nesting properties predicted by band structure calculations [36], at least the transition metal electronic states are expected to change across the CDW transition. Hence we considered it important to carry out bulk-sensitive HAXPES [40,41] of $R_3Co_4Sn_{13}$. Further, in the recent study of Otomo *et al.* [27], using hard x-ray fluorescence spectroscopy across the Ce L_3 edge and Co K edge, the authors concluded there is negligible temperature dependence for the Ce L_3-edge spectrum, but showed that Co K-edge spectra changed across the CDW transition [27]. In the present study, we address this important issue regarding temperature dependent changes in electronic structure for $Ce_3Co_4Sn_{13}$ by investigating the Ce $3d$, Co $2p$, and Sn $3p$ core levels as well as the occupied valence band using bulk-sensitive HAXPES, and the unoccupied conduction band states using XAS.

II. SAMPLE PREPARATION, CHARACTERIZATION, AND EXPERIMENTAL DETAILS

Single crystals of $Ce_3Co_4Sn_{13}$ were synthesized using a Sn-flux method as reported earlier [26]. The samples were characterized for the known cubic crystal structure at room temperature using x-ray diffraction. Electrical resistivity measurements confirmed the metal-to-metal transition at $T_{CDW} \sim 160$ K, associated with the CDW transition [25]. The sample showed a residual resistivity ratio $\text{RRR}(\rho_{300\,\text{K}}/\rho_{10\,\text{K}}) \sim 1.47$, consistent with the value reported earlier in Ref. [25]. Temperature dependent ($T = 20$ and 170 K, i.e. below and above the CDW transition) bulk-sensitive HAXPES ($h\nu \sim 6.5$ keV) was carried out at the Taiwan beamline BL12XU at SPring-8, Japan. The energy calibration (accuracy of ± 10 meV) and

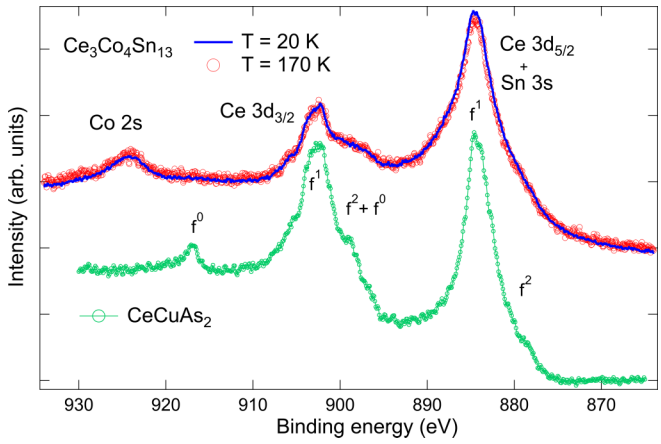

FIG. 1. Ce $3d$ HAXPES core level spectrum measured at $T = 20$ and 170 K showing negligible changes across the CDW transition at $T_{CDW} \sim 160$ K. The labels f^0, f^1, and f^2 mark the final states as observed in $CeCuAs_2$ which is a Kondo system. The f^0 feature shows negligible intensity in $Ce_3Co_4Sn_{13}$.

total energy resolution (270 meV) for the HAXPES measurements were determined from measurements of the Fermi level (E_F) of gold film before and after the experiments. Clean sample surfaces were obtained by cleaving the $Ce_3Co_4Sn_{13}$ crystal in ultrahigh vacuum (UHV). Samples were aligned in a grazing incidence (∼5°) and normal emission geometry for HAXPES experiments. XAS measurements were carried out using normal incidence linearly polarized x rays in the total electron yield (TEY) mode at BL-11A while partial fluorescence yield (PFY) mode measurements were carried out at the BL-08B1 beamline of the Taiwan Light source (TLS), National Synchrotron Radiation Research Center, Taiwan. For the XAS measurements, the samples were mounted with the [110] axis along the surface normal and with incident polarization vector E parallel to [001]. However, since the samples were cleaved in vacuum to obtain clean and reliable XAS spectra, the cleaving resulted in nonuniform surfaces. After cleaving the surfaces, we checked for spectral changes by varying the incidence angle, from normal incidence to 60° away from normal incidence. The spectra showed hardly any changes in spectral shape as a function of incidence angle. Temperature dependent XAS spectra were recorded for the Ce $M_{4,5}$ and Co $L_{2,3}$ edges. The energy resolutions at the Ce $M_{4,5}$ edge and Co $L_{2,3}$-edge were ∼0.2 eV in TEY mode and about 0.45 eV in PFY mode. The Co L_3 edge (∼781 eV) of CoO and the Ni L_2 edge (∼870 eV) of NiO (since the Ni L_2 edge is very close to the Ce M_5 edge) were used as references for accurate energy calibration for Co and Ce edge XAS data, respectively.

III. RESULTS AND DISCUSSION

Figure 1 shows the Ce $3d$ core level spectra measured using HAXPES at temperatures $T = 20$ and 170 K, above and below the CDW transition at $T_{CDW} \sim 160$ K. The spectra show multiple features over the binding energy (BE) range of ∼874 to ∼930 eV and we assign their origins in the following. The Ce $3d_{5/2}$ main peak occurs at 884.6 eV binding energy (BE) and the Ce $3d_{3/2}$ main peak at 902.6 eV BE. The spectra also show other features at ∼898.4 and 924.6 eV. Based on the Gunnarsson-Schonhammer model, it is well known that Ce systems showing the Kondo effect exhibit three features each in the Ce $3d_{5/2}$ and $3d_{3/2}$ energy ranges, namely the f^0, f^1, and f^2 final state features [42–44]. As a reference, we show the Ce $3d$ core level spectra of $CeCuAs_2$, a material which shows the f^0, f^1, and f^2 spectral signatures of Kondo screening [45]. For $Ce_3Co_4Sn_{13}$, we find that the Ce $3d$ spectra show only the f^1 and f^2 features, and the highest BE Ce $3d_{3/2}$ f^0 feature expected at ∼917 eV is missing. This is consistent with the earlier soft x-ray photoemission study of $Ce_3Co_4Sn_{13}$ [38,39]. The feature at ∼924 eV BE is the Co $2s$ core level. In fact, the relative intensity ratio for the $3d_{5/2}$:$3d_{3/2}$ main peaks is also significantly larger in $Ce_3Co_4Sn_{13}$ compared to $CeCuAs_2$. This gave us a hint to check for other core level peaks occurring at the same energy, and indeed we find that the Sn $3s$ core level is expected at 884.7 eV BE [46]. It overlaps with the Ce $3d_{5/2}$ main peak and results in the anomalous intensity ratio being larger than the 3:2 ratio expected from the degeneracy of the levels. The feature at ∼898 eV is assigned to the $3d_{3/2}$ f^2 feature, as the $3d_{5/2}$ f^0 feature should also be suppressed like the $3d_{3/2}$ counterpart.

The negligible intensity of the f^0 feature is known to occur in other systems and is an indicator of reduced hybridization and an increase of the attractive core hole potential [43,44]. It was shown for the quantum critical system $CeCu_{6-x}Au_x$ that the f^0 feature gets suppressed for $x \geqslant 0.2$ and corresponds to a breakdown of Kondo screening, leading to the formation of local moments [44]. The f-electron count changes from $n_f = 0.95$ for $x \leqslant 0.1$ to $n_f = 0.99$ for $x \geqslant 0.2$, i.e., it becomes very close to a pure Ce^{3+} configuration. This also leads to absence of the f^1 final state feature in XAS [47]. Our results confirm the expected behavior in the Ce $M_{4,5}$-edge XAS spectrum, which matches well with a pure atomic Ce^{3+} calculated spectrum, as discussed later (see Fig. 4). In addition, the spectra show negligible temperature dependent changes between $T = 20$ K and $T = 170$ K (Fig. 1), across the CDW transition at $T_{CDW} \sim 160$ K. This is also consistent with the soft x-ray photoemission study of Ce $3d$ core level spectra [38,39].

Figure 2 shows the Sn $3p$ and Co $2p$ core level spectra measured using HAXPES at $T = 20$ and 170 K. Panel (a) shows that the Sn $3p_{3/2}$ level exhibits a main peak at 714.5 eV BE while the $3p_{1/2}$ level shows a main peak at 756.5 eV BE. The main peaks show two satellites with equal energy separation (labeled with asterisks) and progressively reduced intensities, i.e., at ∼14.5 and ∼29 eV from the main peaks. These are assigned to bulk plasmon features. For the Co $2p$ spectra, the Co $2p_{3/2}$ level shows a main peak at 778 eV BE and the $2p_{1/2}$ level shows a main peak at 793 eV BE. The BEs of the Co 2p spectrum match fairly well with reported values of Co in intermetallic systems [48–50]. Since the BE separation between Co $2p_{3/2}$ and Co $2p_{1/2}$ is very close to the plasmon energy, the Co $2p_{3/2}$ plasmon is hidden under the Co $2p_{1/2}$ peak, while for the Co $2p_{1/2}$ peak a weak satellite is observed at 807 eV (labeled with circled asterisks), i.e., at an energy separation of ∼14.5 eV from the main peak, and confirms its plasmon character.

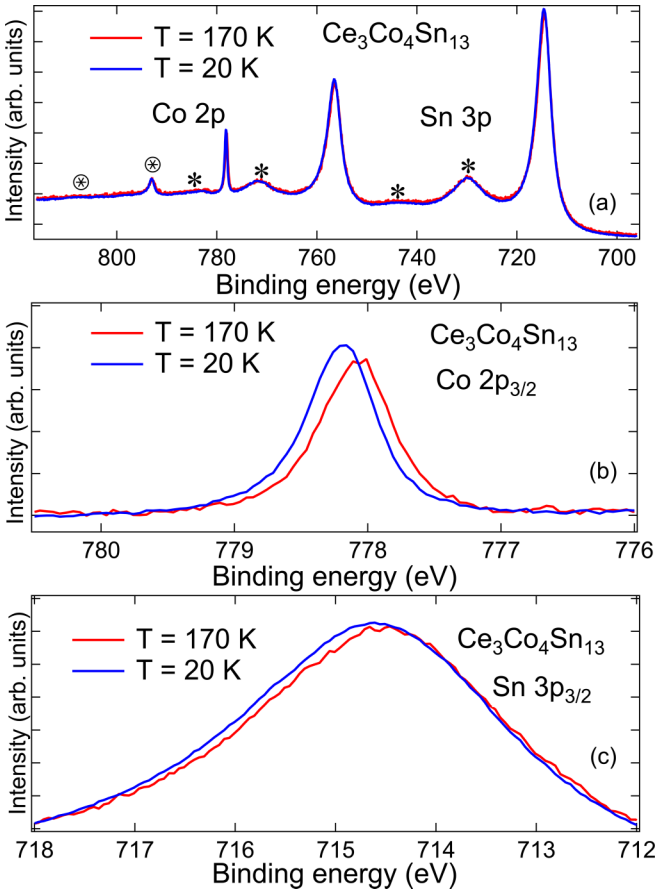

FIG. 2. (a) Co $2p$ and Sn $3p$ HAXPES core level spectra measured at $T = 20$ and 170 K and normalized for area under the curve. (b) Co $2p_{3/2}$ spectrum expanded on the binding energy scale to show clear changes across the CDW transition at $T_{CDW} \sim 160$ K. (c) Sn $3p_{3/2}$ spectrum expanded on the binding energy scale to show small changes across the CDW transition at $T_{CDW} \sim 160$ K.

Figure 2(b) shows the Co $2p_{3/2}$ peak on an expanded scale at $T = 20$ and 170 K. We observe clear changes for the two spectra, with a shift of about 110 meV to higher BE in the $T = 20$ K spectrum compared to the $T = 170$ K spectrum. However, the peak widths show hardly any change. Similarly the Sn $3p_{3/2}$ peak, which is fairly broad, also shows a similar behavior with a shift to 100 meV higher BE but hardly any change in the peak widths. This is in contrast to expectations of a system undergoing a CDW transition, as typical CDW transitions show a broadening or splitting of core level peaks of metal atoms which are involved in the CDW transition [51–54]. The results suggest a very weak charge disproportionation across the CDW transition in $Ce_3Co_4Sn_{13}$, although superstructure peaks were reported in diffraction studies [27].

We next discuss the HAXPES valence band spectra of $Ce_3Co_4Sn_{13}$ measured at 20 and 170 K and shown in Fig. 3. The spectra are normalized for the area under the curve over the plotted energy range. The spectra show two main broad features: from E_F to about 5 eV BE and from 5 to 10 eV BE, with a dip at 5 eV BE. Based on band structure calculations [36], the broad feature between 5 to 10 eV BE is assigned

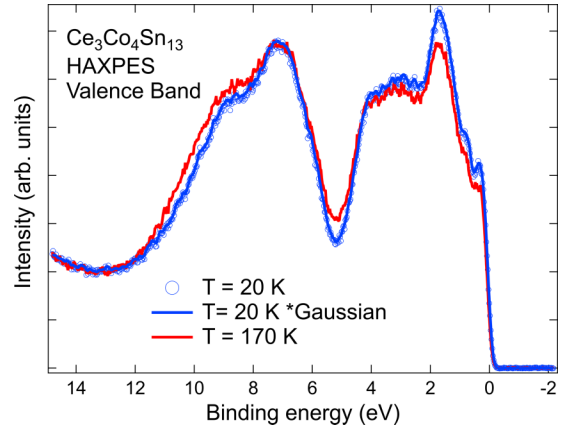

FIG. 3. HAXPES Valence band spectra measured at $T = 20$ and 170 K and normalized for the area under the curve. The $T = 20$ K spectrum convoluted by a Gaussian function of 70 meV FWHM to simulate the thermal broadening is overlaid (line) on the raw data (circles). The data show evidence for sharpening of the Co $3d$ feature at about 2 eV binding energy as well states within 0.5 eV of the Fermi level in the 20 K spectrum compared to the 170 K spectrum.

to dominantly Sn $5s$ and Co $4s$ states, which have a high cross section for HAXPES. The broad feature between E_F and 5 eV BE consists of multiple character states: Sn $5p$ states are spread over the full range, while the Co $3d$ states dominate the feature centered at 1.8 eV BE. It is important to note that there is a small feature just below E_F and within 0.5 eV BE, which is slightly enhanced and more clear in the $T = 20$ K spectrum. We have carried out a simple Gaussian broadening due to temperature increase from 20 to 170 K ($4k_BT \sim 60$ meV at 170 K) by convoluting the $T = 20$ K spectrum with a Gaussian of 60 meV and overlaid (line) on the raw data (symbols) in Fig. 3. As expected, the broadening does not smear out the small feature extending up to 0.5 eV BE. This feature is assigned to Ce $4f$ states, which occurs just at and above E_F in band structure calculations [36]. This small feature straddling the E_F is considered responsible for the enhanced specific heat coefficient reported at low temperatures below 5 K [23]. Here we note that the Ce $4f$ cross section using hard x rays of 6.5 KeV is very low compared to soft x rays [55], and hence the Ce $4f$ states are hardly visible in HAXPES measurements. This was shown recently by comparing the HAXPES valence band spectra of LaTe and CeTe, where, in addition to HAXPES measurements, $3d$-$4f$ resonant photoemission spectroscopy was used to confirm this assignment [56].

Figure 4 shows the Ce $M_{4,5}$-edge XAS of $Ce_3Co_4Sn_{13}$ measured at 170 K using the TEY and PFY modes. Although the resolution is lower in PFY (~0.45 eV) compared to TEY (~0.2 eV), we get the advantage of more bulk sensitivity in PFY spectra. Their comparison shows small differences in relative intensities, and the features are smeared in the PFY spectrum. The experimental TEY data are also compared with a Ce^{3+} multiplet calculation in Fig. 4 using the CTM4XAS program [57]. We obtain good agreement using the broadening values as determined by Thole *et al.* [58], i.e., the M_5 edge is broadened with a Lorentzian of 0.2 eV FWHM, and for the M_4 edge we use a Lorentzian of 0.4 eV FWHM with a

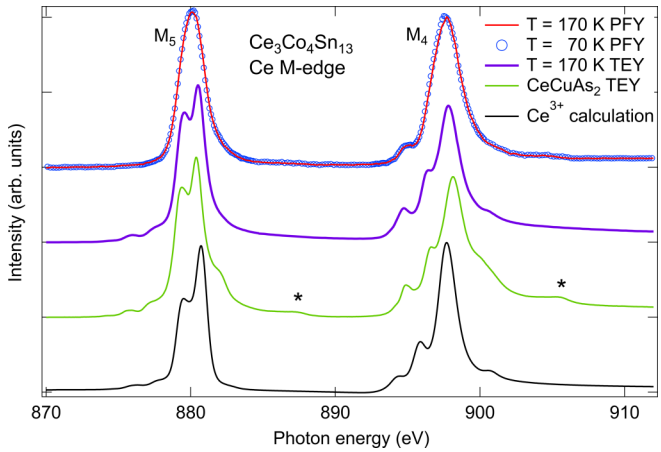

FIG. 4. Ce $M_{4,5}$-edge XAS measured using TEY mode (170 K) and PFY mode (70 and 170 K). For comparison with a system showing Kondo screening, we also plot the Ce $M_{4,5}$-edge spectrum of a reference compound $CeCuAs_2$ which shows the f^1 feature (asterisk marks), which is missing in $Ce_3Co_4Sn_{13}$. The $Ce_3Co_4Sn_{13}$ spectra match fairly well with a Ce^{3+} atomic multiplet calculation. The PFY data show negligible changes as a function of temperature.

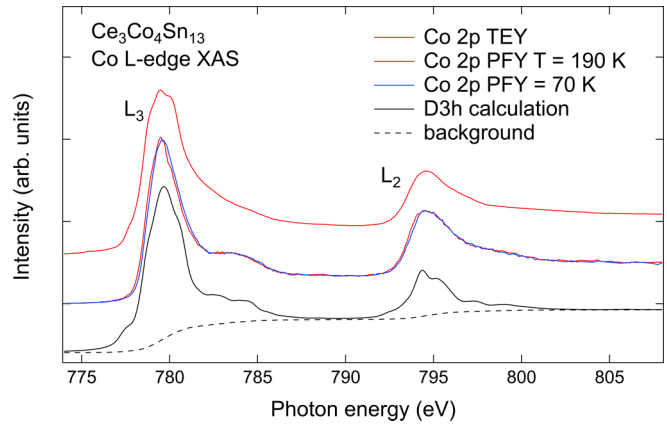

FIG. 5. Co $L_{2,3}$-edge XAS measured using TEY mode (170 K) and PFY mode (70 and 190 K). The TEY and PFY spectra are quite similar except for the hump feature between 783–785 eV photon energy, which is clearly identified in the PFY spectra. The experimental spectra match fairly well with a $CoSn_6$ cluster calculation. A small but finite shift (∼100 meV) to higher photon energy of the PFY spectrum at $T = 70$ K compared to the $T = 190$ K spectrum can be discerned in the data. See Fig. 6 for expanded scale spectra across $T_{CDW} \sim 160$ K.

Fano asymmetry factor of 8. We added a 10% contribution of the $4f_{7/2}$ excited state to account for the combined effects of the crystal field and charge transfer. It is noted that, while the calculations reproduce all the features, the relative intensity of the M_4 derived weak multiplets compared to the main M_4 peak are slightly higher in the experiment. This is suggestive of weak saturation effects due to the low penetration depths of about 20 nm at the Ce $M_{4,5}$ edge. We have also checked that the same calculated spectrum plotted with a Gaussian broadening of 0.45 eV full width at half maximum matches fairly well with the PFY data. In Fig. 4, we also plot the XAS spectrum using TEY mode for $CeCuAs_2$ as a reference material showing the Kondo screening f^1 feature (labeled by asterisks). The f^1 feature has <2% spectral weight in $CeCuAs_2$ [37] and the corresponding weight for $Ce_3Co_4Sn_{13}$ is even lower (<1%). The f^1 feature in XAS originates from the f^0 contribution in the ground state and its negligible spectral weight is consistent with the corresponding negligible f^0 intensity in the Ce 3d core level HAXPES spectrum. Further, the $T = 170$ K and $T = 70$ K spectra show negligible changes as a function of temperature across the CDW transition. Thus, the results are consistent with the Ce 3d HAXPES spectra and indicate that the Ce-derived electronic states do not participate in the transition.

We then measured the Co $L_{2,3}$-edge ($2p$-$3d$) XAS to check for details as a function of temperature using PFY and TEY modes. Figure 5 shows the Co L-edge experimental XAS plotted over a wide energy range covering the L_3 and L_2 range. It is known that PFY spectra can deviate from a genuine x-ray absorption spectrum as measured by TEY or Auger electron yield spectra due to self-absorption, saturation, or if the fluorescence decay rate is not equal for all the final states created in the absorption process [59–61]. This often leads to a relative increase of the higher lying multiplets and the spin-orbit split features compared to the main peak in XAS. We have followed an empirical method [62–64] to compensate for the deviations in the PFY spectrum observed in Co $L_{2,3}$-edge data. The method uses a measurement of the TEY and PFY spectra of the sample under identical conditions. The absorption coefficient can be approximated as [62–64] $\mu(E) = A\mu_F(E)/[B - \mu_F(E)]$ where $\mu_F(E)$ is the PFY spectrum and A and B are constants. The measured PFY spectrum $[\mu_F(E)]$ is then fitted by varying parameters A and B to the corresponding TEY spectrum given by $\mu(E)$. The corrected PFY spectra are plotted in Fig. 5 along with the TEY spectrum. The estimated error bar of this procedure is <10% in the relative intensity of the spectral features. It is noted that the Ce $M_{4,5}$-edge PFY data discussed earlier did not show significant deviations compared to the TEY data, and hence did not need this correction.

The satellite or hump structure to the main Co L_3 peak, positioned at 783–785 eV photon energy, is resolved only in the PFY spectrum in spite of the lower energy resolution. We attribute this to the bulk sensitivity of PFY measurements. The experimental spectrum is compared with a spectrum calculated using the QUANTY code [65–67] for a $Co^{3+}Sn_6$ cluster in a trigonal prism geometry, corresponding to the known structure at room temperature [23,35]. Cluster calculations of the spectra were carried out by varying the electronic parameters in order to match with experiment. For the best match shown in Fig. 5, the charge transfer energy $\Delta = 1.0$ eV and the on-site Coulomb energy $U_{dd} = 5.0$. The relatively large value of U_{dd} compared to Δ classifies $Ce_3Co_4Sn_{13}$ as a strongly correlated charge transfer metal in the Zaanen-Sawatzky-Allen scheme [68]. The trigonal prismatic geometry of $CoSn_6$ leads to a crystal field splitting with three states: a highest energy doublet $e_{g'}$ (d_{yz}, d_{zx}), an intermediate singlet a_{1g} ($d_{3z^2-r^2}$), and the lowest energy doublet $e_{g''}$ (d_{xy}, $d_{x^2-y^2}$) states [69]. Here we note that the a_{1g} and $e_{g''}$ levels can be nearly degenerate or even inverted, depending on the valency as well as the spin-orbit interaction of the Co ion. By

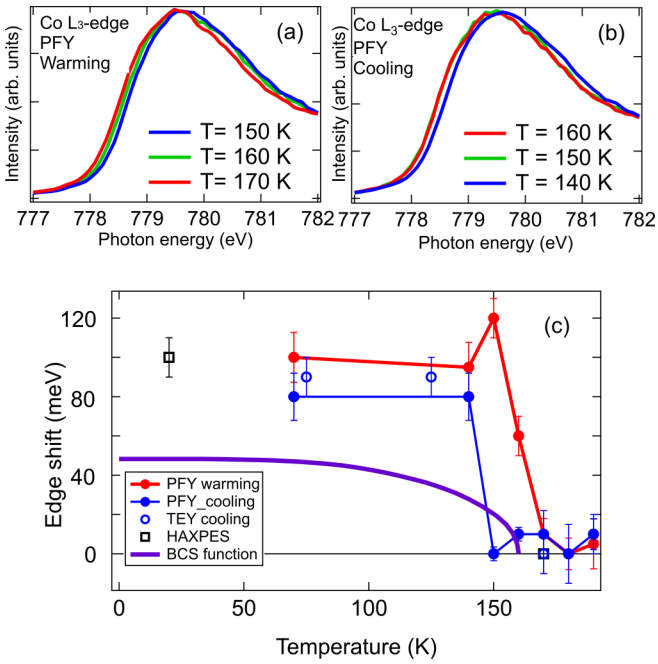

FIG. 6. (a) Co L_3-edge main peak PFY spectra measured at $T = 150$, 160, and 170 K showing the shift across T_{CDW} during warming across the CDW transition (b) Similarly, Co L_3-edge main peak PFY spectra measured at $T = 160$, 150, and 140 K showing the shift across T_{CDW} while cooling across the CDW transition. (c) The relative energy shifts extracted from the XAS and HAXPES spectra across $T_{CDW} \sim 160$ K.

comparing calculations with XAS spectra, it was shown that for the case of Co^{2+} in Ca_3CoRhO_6 the a_{1g} state was the lowest energy level, while for Co^{3+} in $Ca_3Co_2O_6$ the $e_{g''}$ state was the lowest energy level [70]. The energy separation between $e_{g'}$ and a_{1g} was taken to be $D_{10} = 0.8$ eV, while the energy separation between a_{1g} and $e_{g''}$ was taken to be $D_{02} = 0.4$ eV and the hybridization strengths of the d levels with the Sn ligand states were set to $V_{a1g} = 0.5$ eV, $V_{eg'} = 1.4$ eV, and $V_{eg''} = 1.4$ eV. The calculated spectrum matches fairly well with the main peak and satellite structure observed in experiment.

We next discuss the temperature dependence of the Co $L_{2,3}$-edge XAS. The spectra measured at $T = 70$ and 170 K (Fig. 5) are quite similar, but we can discern a small finite shift of ~100 meV in the spectra for the L_3 and L_2 edges. In order to check the detailed temperature dependence of the spectral shift, we measured the Co L_3 and L_2 edges using PFY across the transition for several temperatures in PFY mode (warming and cooling cycle) between 70 and 190 K. For a few temperatures, we also measured the TEY mode while cooling across the transition. The temperature dependent PFY and TEY measurements showed reproducible spectra after the cycling. The spectra are very similar in shape for all the temperatures (not shown), quite like the spectra shown in Fig. 5 for $T = 70$ and 170 K. However, the leading edge shifts as a function of temperature across the CDW transition at $T_{CDW} \sim 160$ K, as shown for the L_3 edge on an expanded scale in Fig. 6. Figure 6(a) shows the PFY spectra across the transition while warming and Fig. 6(b) shows PFY spectra across the transition while cooling.

From the full data set measured between 70 and 190 K, we extracted the relative leading edge shifts as a function of temperature in the warming and cooling cycle, and the data are plotted in Fig. 6(c). The data clearly show that the shifts exhibit a hysteresis in the warming and cooling cycle. The hysteresis matches with the hysteresis seen in the specific heat data of Lue *et al.* [25]. This confirms that the transition is a first-order transition, as was concluded by Lue *et al.* [25]. In contrast, a recent study by Otomo *et al.* carried out at the Co K edge using x-ray fluorescence spectroscopy concluded a second-order transition. While we do not understand the origin of the difference between the present Co $L_{2,3}$-edge data compared to the Co K-edge data of Otomo *et al.*, the comparatively higher energy resolution at the Co $L_{2,3}$ edge allows us to probe the $2p$-$3d$ excitations in a reliable way. Further, the shifts of ~100 meV seen in Co $2p$ HAXPES spectra are also plotted in the same figure and are consistent with the Co $L_{2,3}$-edge XAS results. In the same figure, we have also plotted the theoretical BCS gap function assuming a weak-coupling transition at $T = 160$ K, which is considered a valid order parameter for a typical Peierls-type CDW transition [4,71]. If the gap formation takes place and it is a second-order BCS type transition, it implies the core levels can also show the same gradual shift as the gap. Here, we are using the comparison just to show that the shift that takes place has a value larger (nearly twice the magnitude at low T) than the BCS expectation, it is not gradual, and it shows a hysteresis. While we do not observe a gap formation in the valence band density of states, and the electrical transport also shows a metal-to-metal transition, it is clear that the theoretical weak-coupling BCS function (assuming $2\Delta/k_BT_{CDW} \sim 3.5$) also does not match the experimentally observed shift in the Co $L_{2,3}$-edge XAS and Co $2p$ HAXPES spectra. Thus, although the energy shift indicates changes across the CDW transition, the results do not follow the BCS expectation, and instead suggest an unusual first-order CDW transition in $Ce_3Co_4Sn_{13}$.

In a recent optical spectroscopy study on $La_3Co_4Sn_{13}$ and $Ce_3Co_4Sn_{13}$, the authors also concluded the absence of a charge density wave gap across T_{CDW}, but observed a spectral weight depletion or pseudogap formation within 0.4 eV coupled to a transfer of spectral weight up to 1 eV in the joint density of states [72]. It is noted that in a recent angle-resolved photoemission spectroscopy study [73] of the classic CDW system $NbSe_3$, which is also coupled to a metal-to-metal transition, it was shown that the momentum resolved electronic structure exhibits gaps occurring at binding energies away from the Fermi level but which are connected by two different incommensurate modulation wave vectors. Further, we have checked that while the Co $2s$ spectra are not conclusive about indicating a shift, the Co $3d$ densities of states do not show a shift like the Co $2p$ core levels and the Co L-edge XAS spectra. Hence a rigid shift of all Co related levels cannot be concluded. While the Ce sites also show structural changes and indicate two distinct sites in the low temperature CDW phase [27], the Ce $3d$ HAXPES and Ce $M_{4,5}$-edge XAS spectra do not show changes across the CDW transition. The absence of a rigid shift could mean that the observed shifts in Co $2p$ core level HAXPES and the Co $L_{2,3}$ edge could be

associated with a change in the core hole Coulomb interaction U_{pd}. However, since we see a similar shift in the Co $2p$ and Sn $3p$ core levels, we believe the results are more consistent with changes in the ground state, as the crystal structure data also involve changes in the Co and Sn sites across the CDW transition [27]. We hope our study motivates further work, specifically using resonant photoemission spectroscopy, resonant inelastic x-ray scattering, and angle-resolved photoemission spectroscopy, on $Ce_3Co_4Sn_{13}$ as well as other systems in the $R_3M_4Sn_{13}$, $R_5M_4Si_{10}$, and RMC_2 series which show CDW transitions coupled to a metal-metal transition.

IV. CONCLUSIONS

In conclusion, temperature dependent HAXPES and XAS were used to investigate the occupied and unoccupied electronic states of $Ce_3Co_4Sn_{13}$. While the Ce derived states do not show any change across the transition, the Co and Sn core level HAXPES spectra show small finite shifts in energy across T_{CDW}. The comparison of the Ce $M_{4,5}$-edge XAS spectrum with calculations indicate a trivalent ionic Ce^{3+} and absence of Kondo screening in $Ce_3Co_4Sn_{13}$, consistent with HAXPES results. The Co $L_{2,3}$-edge XAS spectrum is consistent with Co^{3+} surrounded by Sn atoms in a trigonal prism coordination. The temperature dependent Co $L_{2,3}$-edge XAS shows that a small shift occurs with a hysteresis across T_{CDW}, indicating a first-order transition. Valence band spectra show that the Co $3d$ states occur away from the Fermi level while the tail of the Ce $4f$ states occurs within 0.5 eV of the Fermi level, with a normal Fermi edge above and below T_{CDW}. The results suggest $Ce_3Co_4Sn_{13}$ exhibits an unusual CDW coupled to a metal-to-metal transition.

ACKNOWLEDGMENT

A.C. thanks the Ministry of Science and Technology of the Republic of China, Taiwan for financially supporting this research under Contracts No. MOST 106-2112-M-213-001-MY2 and No. MOST 106-2112-M-006-013-MY3.

[1] R. E. Peierls, *Quantum Theory of Solids* (Oxford University Press, New York, 1955).
[2] W. Fogle and J. H. Perlstein, Phys. Rev. B **6**, 1402 (1972).
[3] P. Monceau, N. P. Ong, A. M. Portis, A. Meerschaut, and J. Rouxel, Phys. Rev. Lett. **37**, 602 (1976).
[4] G. Gruner, Rev. Mod. Phys. **60**, 1129 (1988).
[5] F. J. Di Salvo, D. E. Moncton, and J. V. Waszczak, Phys. Rev. B **14**, 4321 (1976).
[6] P. Aebi, Th. Pillo, H. Berger, and F. Lévy, J. Electron Spectrosc. Relat. Phenom. **117-118**, 433 (2001).
[7] K. Rossnagel, J. Phys.: Condens. Matter **23**, 213001 (2011).
[8] T. Kiss, T. Yokoya, A. Chainani, S. Shin, T. Hanaguri, M. Nohara, and H. Takagi, Nat. Phys. **3**, 720 (2007).
[9] H. Cercellier, C. Monney, F. Clerc, C. Battaglia, L. Despont, M. G. Garnier, H. Beck, P. Aebi, L. Patthey, H. Berger, and L. Forro, Phys. Rev. Lett. **99**, 146403 (2007).
[10] H. Sato, S. Tajima, H. Takagi, and S. Uchida, Nature (London) **338**, 241 (1989).
[11] A. P. Ramirez, P. Schiffer, S-W. Cheong, C. H. Chen, W. Bao, T. T. M. Palstra, P. L. Gammel, D. J. Bishop, and B. Zegarski, Phys. Rev. Lett. **76**, 3188 (1996).
[12] M. Medarde, M. T. Fernandez-Diaz, and Ph. Lacorre, Phys. Rev. B **78**, 212101 (2008).
[13] G. Ghiringhelli, M. Le Tacon, M. Minola, S. Blanco-Canosa, C. Mazzoli, N. B. Brookes, G. M. De Luca, A. Frano, D. G. Hawthorn, F. He, T. Loew, M. Moretti Sala, D. C. Peets, M. Salluzzo, E. Schierle, R. Sutarto, G. A. Sawatzky, E. Weschke, B. Keimer, and L. Braicovich, Science **337**, 821 (2012).
[14] J. Chang, E. Blackburn, A. T. Holmes, N. B. Christensen, J. Larsen, J. Mesot, R. Liang, D. A. Bonn, W. N. Hardy, A. Watenphul, M. V. Zimmermann, E. M. Forgan, and S. M. Hayden, Nat. Phys. **8**, 871 (2012).
[15] S. Gerber, H. Jang, H. Nojiri, S. Matsuzawa, H. Yasumura, D. A. Bonn, R. Liang, W. N. Hardy, Z. Islam, A. Mehta, S. Song, M. Sikorski, D. Stefanescu, Y. Feng, S. A. Kivelson, T. P. Devereaux, Z.-X. Shen, C.-C. Kao, W.-S. Lee, D. Zhu, and J.-S. Lee, Science **350**, 949 (2015).
[16] A. Sacchetti, E. Arcangeletti, A. Perucchi, L. Baldassarre, P. Postorino, S. Lupi, N. Ru, I. R. Fisher, and L. Degiorgi, Phys. Rev. Lett. **98**, 026401 (2007).
[17] V. Brouet, W. L. Yang, X. J. Zhou, Z. Hussain, R. G. Moore, R. He, D. H. Lu, Z. X. Shen, J. Laverock, S. B. Dugdale, N. Ru, and I. R. Fisher, Phys. Rev. B **77**, 235104 (2008).
[18] N. Ru, J.-H. Chu, and I. R. Fisher, Phys. Rev. B **78**, 012410 (2008).
[19] K. Y. Shin, J. Laverock, Y. Q. Wu, C. L. Condron, M. F. Toney, S. B. Dugdale, M. J. Kramer, and I. R. Fisher, Phys. Rev. B **77**, 165101 (2008).
[20] J.-S. Kang, D. H. Kim, H. J. Lee, J. Hwang, H.-K. Lee, H.-D. Kim, B. H. Min, K. E. Lee, Y. S. Kwon, J. W. Kim, K. Kim, B. H. Kim, and B. I. Min, Phys. Rev. B **85**, 085104 (2012).
[21] E. Lee, D. H. Kim, J. D. Denlinger, J. Kim, K. Kim, B. I. Min, B. H. Min, Y. S. Kwon, and J.-S. Kang, Phys. Rev. B **91**, 125137 (2015).
[22] C. Israel, E. M. Bittar, O. E. Aguero, R. R. Urbano, C. Rettori, I. Torriani, P. G. Pagliuso, N. O. Moreno, J. D. Thompson, M. F. Hundley, J. L. Sarrao, and H. A. Borges, Physica B (Amsterdam) **359-361**, 251 (2005).
[23] E. L. Thomas, H.-O. Lee, A. N. Bankston, S. MaQuilon, P. Klavins, M. Moldovan, D. P. Young, Z. Fisk, and J. Y. Chan, J. Solid State Chem. **179**, 1642 (2006).
[24] M. A. Pires, L. M. Ferreira, J. G. S. Duque, R. R. Urbano, O. Agüero, I. Torriani, C. Rettori, E. M. Bittar, and P. G. Pagliuso, J. Appl. Phys. **99**, 08J311 (2006).
[25] C. S. Lue, H. F. Liu, S.-L. Hsu, M. W. Chu, H. Y. Liao, and Y. K. Kuo, Phys. Rev. B **85**, 205120 (2012)
[26] H. F. Liu, C. N. Kuo, C. S. Lue, K.-Z. Syu, and Y. K. Kuo, Phys. Rev. B **88**, 115113 (2013).
[27] Y. Otomo, K. Iwasa, K. Suyama, K. Tomiyasu, H. Sagayama, R. Sagayama, H. Nakao, R. Kumai, and Y. Murakami, Phys. Rev. B **94**, 075109 (2016).
[28] R. N. Shelton, L. S. Hausermann-Berg, P. Klavins, H. D. Yang, M. S. Anderson, and C. A. Swenson, Phys. Rev. B **34**, 4590 (1986).

[29] H. D. Yang, P. Klavins, and R. N. Shelton, Phys. Rev. B **43**, 7688 (1991).

[30] K. Ghosh, S. Ramakrishnan, and G. Chandra, Phys. Rev. B **48**, 4152 (1993).

[31] F. Galli, S. Ramakrishnan, T. Taniguchi, G. J. Nieuwenhuys, J. A. Mydosh, S. Geupel, J. Lüdecke, and S. van Smaalen, Phys. Rev. Lett. **85**, 158 (2000).

[32] Y. K. Kuo, F. H. Hsu, H. H. Li, H. L. Huang, C. W. Huang, C. S. Lue, and H. D. Yang, Phys. Rev. B **67**, 195101 (2003).

[33] M. Murase, A. Tobo, H. Onodera, Y. Hirano, T. Hosaka, S. Shimomura, and N. Wakabayashi, J. Phys. Soc. Jpn. **73**, 2790 (2004).

[34] M. Roman, J. Strychalska-Nowak, T. Klimczuk, and K. K. Kolincio, Phys. Rev. B **97**, 041103(R) (2018).

[35] I. W. H. Oswald, B. K. Rai, G. T. McCandless, E. Morosan, and J. Y. Chan, CrystEngComm **19**, 3381 (2017).

[36] G. Zhong, X. Lei, and J. Mao, Phys. Rev. B **79**, 094424 (2009).

[37] K. Iwasa, Y. Otomo, K. Suyama, K. Tomiyasu, S. Ohira-Kawamura, K. Nakajima, and J. M. Mignot, Phys. Rev. B **95**, 195156 (2017).

[38] A. Slebarski, B. D. White, M. Fijalkowski, J. Goraus, J. J. Hamlin, and M. B. Maple, Phys. Rev. B **86**, 205113 (2012).

[39] A. Slebarski and J. Goraus, Phys. Rev. B **88**, 155122 (2013).

[40] C. S. Fadley, J. Electron Spectrosc. Relat. Phenom. **190**, 165 (2013).

[41] *Hard X-ray Photoelectron Spectroscopy (HAXPES)*, Springer Series in Surface Sciences Vol. 59, edited by J. C. Woicik (Springer International, Cham, Switzerland, 2016).

[42] O. Gunnarsson and K. Schonhammer, Phys. Rev. Lett. **50**, 604 (1983).

[43] J. C. Fuggle, F. U. Hillebrecht, Z. Zolnierek, R. Lasser, Ch. Freiburg, O. Gunnarsson, and K. Schonhammer, Phys. Rev B **27**, 7330 (1983).

[44] M. Klein, J. Kroha, H. V. Löhneysen, O. Stockert, and F. Reinert, Phys. Rev. B **79**, 075111 (2009).

[45] A. Chainani, M. Matsunami, M. Taguchi, R. Eguchi, Y. Takata, M. Oura, S. Shin, K. Sengupta, E. V. Sampathkumaran, Th. Doert, Y. Senba, H. Ohashi, K. Tamasaku, Y. Kohmura, M. Yabashi, and T. Ishikawa, Phys. Rev. B **89**, 235117 (2014).

[46] J. F. Moulder, W. F. Stickle, P. E. Sobol, and K. D. Bomben, *Handbook of X-Ray Photoelectron Spectroscopy* (Physical Electronics, Eden Prairie, MN, 1995).

[47] J. C. Fuggle, F. U. Hillebrecht, J.-M. Esteva and R. C. Karnatak, O. Gunnarsson, and K. Schonhammer, Phys. Rev. B **27**, 4637 (1983).

[48] S. Ouardi, G. H. Fecher, B. Balke, A. Beleanu, X. Kozina, G. Stryganyuk, C. Felser, W. Kloss, H. Schrader, F. Bernardi, J. Morais, E. Ikenaga, Y. Yamashita, S. Ueda, and K. Kobayashi, Phys. Rev. B **84**, 155122 (2011).

[49] J. Barth, G. H. Fecher, B. Balke, S. Ouardi, T. Graf, C. Felser, A. Shkabko, A. Weidenkaff, P. Klaer, H. J. Elmers, H. Yoshikawa, S. Ueda, and K. Kobayashi, Phys. Rev. B **81**, 064404 (2010).

[50] V. Alijani, S. Ouardi, G. H. Fecher, J. Winterlik, S. S. Naghavi, X. Kozina, G. Stryganyuk, C. Felser, E. Ikenaga, Y. Yamashita, S. Ueda, and K. Kobayashi, Phys. Rev. B **84**, 224416 (2011).

[51] N. V. Smith, S. D. Kevan, and F. J. DiSalvo, J. Phys. C **18**, 3175 (1985).

[52] H.-J. Noh, E.-J. Cho, H.-D. Kim, J.-Y. Kim, C.-H. Min, B.-G. Park, and S.-W. Cheong, Phys. Rev. B **76**, 233106 (2007).

[53] K. Ishizaka, T. Kiss, T. Yamamoto, Y. Ishida, T. Saitoh, M. Matsunami, R. Eguchi, T. Ohtsuki, A. Kosuge, T. Kanai, M. Nohara, H. Takagi, S. Watanabe, and S. Shin, Phys. Rev. B **83**, 081104(R) (2011).

[54] K.-T. Ko, H.-H. Lee, D.-H. Kim, J.-J. Yang, S.-W. Cheong, M. J. Eom, J. S. Kim, R. Gammag, K.-S. Kim, H.-S. Kim, T.-H. Kim, H.-W. Yeom, T.-Y. Koo, H.-D. Kim, and J.-H. Park, Nat. Commun. **6**, 7342 (2015).

[55] J. J. Yeh and I. Lindau, At. Data Nucl. Data Tables **32**, 1 (1985).

[56] A. Chainani, M. Oura, M. Matsunami, A. Ochiai, T. Takahashi, Y. Tanaka, K. Tamasaku, Y. Kohmura, and T. Ishikawa J. Electron Spectrosc. Relat. Phenom. **208**, 116 (2016).

[57] E. Stavitski and F. M. F. de Groot, Micron **41**, 687 (2010).

[58] B. T. Thole, G. van der Laan, J. C. Fuggle, G. A. Sawatzky, R. C. Karnatak, and J.-M. Esteva, Phys. Rev. B **32**, 5107 (1985).

[59] F. M. F. de Groot, M. A. Arrio, Ph. Sainctavit, Ch. Cartier, and C. T. Chen, Solid State Commun. **92**, 991 (1994).

[60] M. Pompa, A. M. Flank, P. Lagarde, J. C. Rife, I. Stekhin, M. Nakazawa, H. Ogasawara, and A. Kotani, Phys. Rev. B **56**, 2267 (1997)

[61] M. Nakazawa, H. Ogasawara, A. Kotani, and P. Lagarde, J. Phys. Soc. Jpn. **67**, 323 (1998).

[62] R. Carboni, S. Giovannini, G. Antonioli, and F. Boscherini, Phys. Scr. T **115**, 986 (2005).

[63] S. Lafuerza, J. Garcia, G. Subias, J. Blasco, J. Herrero-Martin, and S. Pascarelli, Phys. Rev. B **90**, 245137 (2014).

[64] V. Cuartero, S. Lafuerza, G. Subias, J. Garcia, E. Schierle, J. Blasco, and J. Herrero-Albillos, Phys. Rev. B **91**, 165111 (2015).

[65] M. W. Haverkort, M. Zwierzycki, and O. K. Andersen, Phys. Rev. B **85**, 165113 (2012).

[66] Y. Lu, M. Hoppner, O. Gunnarsson, and M. W. Haverkort, Phys. Rev. B **90**, 085102 (2014).

[67] M. Haverkort, G. Sangiovanni, P. Hansmann, A. Toschi, Y. Lu, and S. Macke, Europhys. Lett. **108**, 57004 (2014).

[68] J. Zaanen, G. A. Sawatzky, and J. W. Allen, Phys. Rev. Lett. **55**, 418 (1985).

[69] R. Huisman, R. de Jonge, C. Haas, and F. Jellinek, J. Solid State Chem. **3**, 56 (1971).

[70] T. Burnus, Z. Hu, H. Wu, J. C. Cezar, S. Niitaka, H. Takagi, C. F. Chang, N. B. Brookes, H.-J. Lin, L. Y. Jang, A. Tanaka, K. S. Liang, C. T. Chen, and L. H. Tjeng, Phys. Rev. B **77**, 205111 (2008).

[71] J. Solyom, Adv. Phys. **28**, 201 (1979).

[72] W. J. Ban, J. L. Luo, and N. L. Wang, J. Phys.: Condens. Matter **29**, 405603 (2017).

[73] C. W. Nicholson, C. Berthod, M. Puppin, H. Berger, M. Wolf, M. Hoesch, and C. Monney, Phys. Rev. Lett. **118**, 206401 (2017).